Large-scale influence of defect bonds in geometrically constrained self-assembly

Bosiljka Tadić,[1,2] Milovan Šuvakov,[3,4] Miroslav Andjelković,[5] and Geoff J. Rodgers[6]
[1]*Department of Theoretical Physics, Jožef Stefan Institute, Jamova 39, Ljubljana, Slovenia*
[2]*Complexity Science Hub Vienna, Josephstadter Strasse 39, Vienna, Austria*
[3]*Institute of Physics, University of Belgrade, Pregrevica 118, 11080 Zemun-Belgrade, Serbia*
[4]*Department of Health Sciences Research, Center for Individualized Medicine, Mayo Clinic, Rochester, Minnesota 55905, USA*
[5]*Department of Thermal Engineering and Energy, Vinca Institute of Nuclear Sciences-National Institute of the Republic of Serbia, University of Belgrade, 11000 Belgrade, Serbia*
[6]*Brunel University London, Uxbridge Middlesex UB8 3PH, United Kingdom*

(Received 7 May 2020; accepted 3 September 2020; published 24 September 2020)

Recently, the importance of higher-order interactions in the physics of quantum systems and nanoparticle assemblies has prompted the exploration of new classes of networks that grow through geometrically constrained simplex aggregation. Based on the model of chemically tunable self-assembly of simplexes [Šuvakov *et al.*, Sci. Rep. **8**, 1987 (2018)], here we extend the model to allow the presence of a defect edge per simplex. Using a wide distribution of simplex sizes (from edges, triangles, tetrahedrons, etc., up to 10-cliques) and various chemical affinity parameters, we investigate the magnitude of the impact of defects on the self-assembly process and the emerging higher-order networks. Their essential characteristics are treelike patterns of defect bonds, hyperbolic geometry, and simplicial complexes, which are described using the algebraic topology method. Furthermore, we demonstrate how the presence of patterned defects can be used to alter the structure of the assembly after the growth process is complete. In the assemblies grown under different chemical affinities, we consider the removal of defect bonds and analyze the progressive changes in the hierarchical architecture of simplicial complexes and the hyperbolicity parameters of the underlying graphs. Within the framework of cooperative self-assembly of nanonetworks, these results shed light on the use of defects in the design of complex materials. They also provide a different perspective on the understanding of extended connectivity beyond pairwise interactions in many complex systems.

DOI: 10.1103/PhysRevE.102.032307

I. INTRODUCTION

In recent years, the application of graph theory to analyze complex patterns in empirical data has revolutionized research in various interdisciplinary sciences. Some well-known examples include emotion-driven online dynamics with co-evolving networks of users and posts [1] and mapping brain imaging data (see recent related Ref. [2] and references therein). However, the use of graphs for mapping certain problems in physics and materials science is still in its infancy [3–8]. In this case, more profound knowledge of the physics and chemistry of the problem helps to appropriately identify the nodes and edges of the structure, which often refers to the phase space of the system rather than a real-space structure.

In materials science, complex structures made of nanoscale objects often correlate with an increased functionality [9,10]. Processes of self-assembly are widely used to grow such systems, where the addition of each object to the growing structure obeys certain rules and locally minimizes the energy [11–13]. In this context, defect morphologies may occur where defects of various types are often used to direct self-assembly and, by analogy with disorder and domain walls in crystalline solids, to alter the physical properties of the system [14–16]. Therefore, the use of mathematical concepts [17] and graph representations—nanonetworks [3]—are highly desirable for both the design and characterization of the nanostructured assemblies. For example, real-space networks are visualized with the nanoparticles as nodes and edges representing a kind of chemical binding [18] or another association between them that is relevant for the problem in question. For example, the network representations of the conducting nanoparticle films have been studied in Refs. [19–21]. The use of graph theory has enabled the description and differentiation of the structures that promote enhanced conduction via single-electron tunnelings between nanoparticles spaced within the quantum tunneling radius in the direction of the current.

Cooperative self-assembly [22–24], where the preformatted group of particles attaches to a growing structure, represents a higher level of the self-assembly processes and opens an avenue towards new types of materials inspired by *mathematics* [17,25]. Colloids with "valence" and directional bonding are a physical reality [26], particles with $n \in [1, 7]$ active patches were created by two-stage swelling of the minimal moment clusters and subsequent DNA functionalization, resulting in different forms as spheres, dumbbells, triangles, tetrahedra, and higher-order structures. In these processes, the geometrical-compatibility constraints of the binding forms

with the growing structure play an important role, apart from the chemical affinity between the structure and the binding nanoparticles. Recently, we developed a model with the appropriate self-assembly rules [25,27], where the building blocks are suitably described by simplexes, i.e., edges, triangles, tetrahedrons, and cliques of higher orders. A prominent feature of these structures is a hierarchical architecture of simplicial complexes, which is accessible to the methods of the algebraic topology of graphs [28,29], as well as emergent hyperbolicity in the graph's metric space [30–34].

In this work, based on the model in Ref. [25], we extend the study of the cooperative self-assembly by considering the presence of defect simplexes and describe the impact of defect bonds on the assembled nanonetworks. Specifically, we show how the presence of simplexes with a defect edge can alter the course of the process leading to a structure with nonrandom patterns of defect bonds and changed topological features of the assembly, depending on the size of the binding simplexes and the chemical affinity parameters. We further demonstrate how the patterned defect bonds can be utilized to alter the structure in the already grown assembly. Changes in the topological properties of the assemblies are quantified using the algebraic topology analysis of simplicial complexes, as well as by determining several graph measures and the hyperbolicity parameter of the underlying graph.

In Sec. II, we present the details of the model and grow several assemblies with defects for further analysis. Section III is devoted to topological analysis of these assemblies as well as assemblies obtained by removal of defect bonds, while in Sec. IV, we determine the Gromov hyperbolicity and other graph parameters of these assemblies. Finally, Sec. V contains a brief summary and discussion of the results.

II. THE MODEL OF COOPERATIVE SELF-ASSEMBLY WITH DEFECTS

Following the original model [25], we consider the assembly of simplexes that are full graphs (cliques) of n vertices. Moreover, with a finite probability, each clique can have a bond that differs from the other bonds, i.e., a defect. Starting from an initial simplex (node), the new simplex of the size driven from the probability $p_n \sim n^{-\alpha}$ ($\alpha = 2$ if not specified) is attached to the growing structure by sharing one of its faces with an existing simplex. Notice that a simplex of n vertices possesses faces as subsimplexes of all orders $q = 0, 1, 2, 3, \ldots, q_{\max} - 1$ from the vertex to the largest subsimplex, where $q_{\max} = n - 1$ indicates the order of the simplex. Determining the face to be shared depends first on the number of geometrically compatible sites in the current structure (geometrical compatibility constraint). The clique is added to the selected docking site by sharing its q-face, as described below; then the remaining $n_a = q_{\max} - q$ vertices are added. All the implicated vertices are linked together to form the clique. The affinity of the system towards the addition of a group n_a is described by the chemical affinity parameter ν [25,35], which modifies the probability defined based on the geometry factor alone [see Eq. (1)]. Specifically, for a large negative ν, the system likes the addition of particles, which results in sharing a minimal face, that is a single node. In this limit, the cliques are effectively repelling each other, whereas in the opposite limit, with a large $\nu > 0$, a single node is preferably added; thus, the added clique shares its largest face with a previous compatible structure [25] [see Figs. 1(a) and 1(b) and text below].

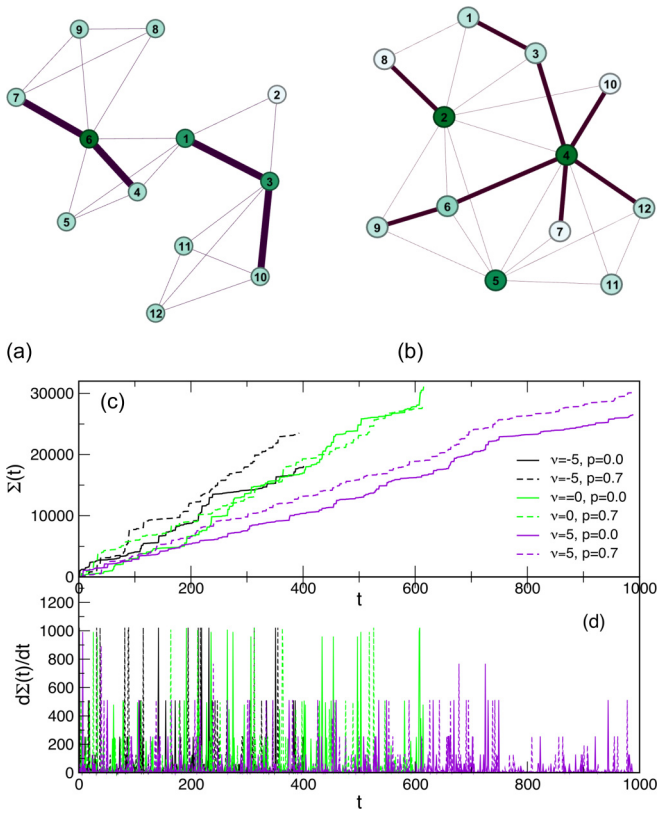

FIG. 1. Illustration of the self-assembly of triangles and tetrahedra with defect bonds until the network size reaches $N(t) = 12$ nodes for (a) large negative $\nu = -5$ and (b) large positive affinity $\nu = +5$. The sequence of events is described in the text. (c) For the distribution of the attaching simplexes in the range $n \in [2, 10]$, the evolution of the number of simplexes and faces $\Sigma(t)$ with time steps t until the number of nodes reaches $N_{\max} = 1000$. Three values of the affinity parameter ν are considered, shown in the legend, combined with the probability $p = 0.7$ of a defect bond in simplexes and simplexes with all pure bonds $p = 0.0$. The corresponding fluctuations in the number of simplexes over time are shown in (d).

Furthermore, the presence of defect bonds affects the attachment, as described in the following. At each evolution step t, the normalized probability that a clique σ of order $q_{\max}$ will attach along its face of order q is determined by the expression

$$p_\sigma(q_{\max}, q; p, t) = \frac{c_q(p,t)e^{-\nu(q_{\max}-q)}}{\sum_{q=0}^{q_{\max}-1} c_q(p,t)e^{-\nu(q_{\max}-q)}}. \quad (1)$$

Here, the factor $c_q(p,t)$ is defined as the number of geometrically compatible sites, i.e., faces of order q on the growing network at time t. It is a subject of the presence of a defect edge, symbolically indicated by p dependence in $c_q(p,t)$, as explained below, and modified by the chemical affinity of the structure to add $n_a = q_{\max} - q$ new nodes controlled by the parameter ν. To compute the number of geometrically similar docking sites $c_q(p,t)$ of the searched order q, in the present model we distinguish between the binding faces with defect

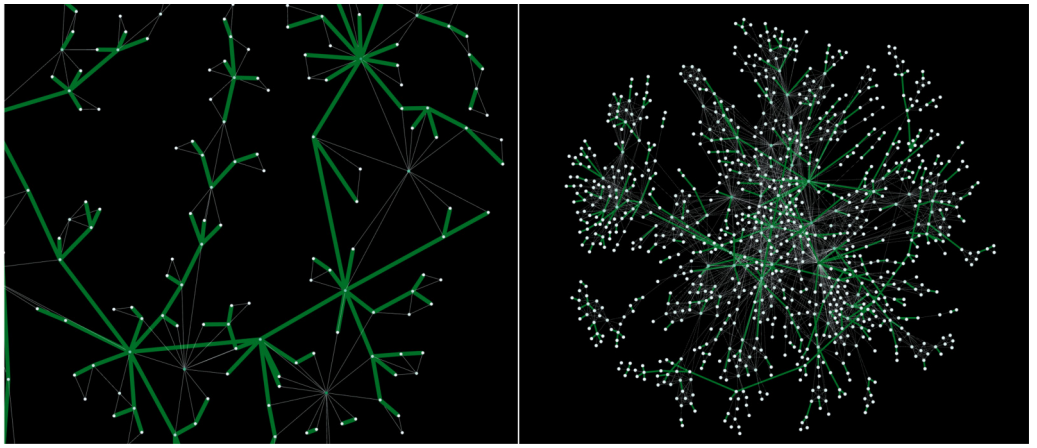

FIG. 2. Close-up of the structure of assembly of triangles (left) and the assembly of the distributed clique sizes $n \in [2, 10]$ according to $\sim n^{-2}$ (right) for strictly geometric aggregation ($\nu = 0$) and 70% defect simplexes, $N_{\max} = 1000$. Defect edges are shown as thick (green) lines.

bonds from those without defects. For this work, we adopt the rule that a face without defect bond of the new clique is shared with the appropriate pure face on the growing structure. Then the defect edge extends from a (preferably defect) node in the docking site towards one of the newly added nodes, which favors the sharing of a defect node. Thus, with each added clique, a new defect bond appears with the fixed probability p. As described below, this process leads to a nonrandom pattern of defect bonds. We consider how this model might be further adapted by changing the attachment rules and parameters in the Discussion below.

To illustrate the assembly process, we show the first few growth steps [starting from a single node until the network size reaches $N(t) = 12$] of the assemblies composed of a mixture of triangles and tetrahedra for $\nu = -5$ and $\nu = +5$, and $p = 1$ [see Figs. 1(a) and 1(b)]. The corresponding simulation output files are displayed below. Specifically, from left to right, are the time step t; number of nodes, $N(t)$; number of simplexes and faces, $\Sigma(t)$; size of the added clique, n; number of the added nodes, n_a; and identity $i_1, i_2, \ldots, i_n$ of nodes belonging to that clique. The bracket (i, j) indicates the defect edge of that clique. In particular, in the assembly with $\nu = +5$, we have the following sequence of events, resulting in the graph in Fig. 1(b):

```
1 3 7 3 2 1 2 3 (1, 3)
2 4 11 3 1 2 3 4 (3, 4)
3 6 23 4 2 2 4 5 6 (4, 6)
4 7 27 3 1 4 5 7 (4, 7)
5 8 31 3 1 1 2 8 (2, 8)
6 9 39 4 1 2 5 6 9 (6, 9)
7 10 43 3 1 2 4 10 (4, 10)
8 12 55 4 2 4 5 11 12 (4, 12)
```

Meanwhile, growth is faster for $\nu = -5$ [see the graph in Fig. 1(a)] because the number of added nodes, n_a, per clique is higher, in particular:

```
1 3 7 3 2 1 2 3 (1, 3)
2 6 21 4 3 1 4 5 6 (4, 6)
3 9 35 4 3 6 7 8 9 (6, 7)
4 12 49 4 3 3 10 11 12 (3, 10)
```

The presence of defects that are already built in the structure affects future binding events. Figure 1 illustrates the impact of the presence of defect edges on the course of the process for varied parameters. For the purpose of this work, we grow a large number of assemblies by varying the size of the building simplexes n and the control parameters ν and p. To control the size of the assembly, growth is stopped when the number of nodes exceeds a given number $N_{\max}$ for the first time. For illustration, some examples of grown assemblies are shown in Fig. 2 and in Fig. 3. The impact of defect edges for a given p also depends on the size and the dispersion of the attaching cliques, and the binding affinity ν. When the affinity among cliques is significant, such that they intend to share their maximal faces, the aggregation of defect edges is more effective, leading to an extended defect structure that further constrains the process. Notably, defect bonds make

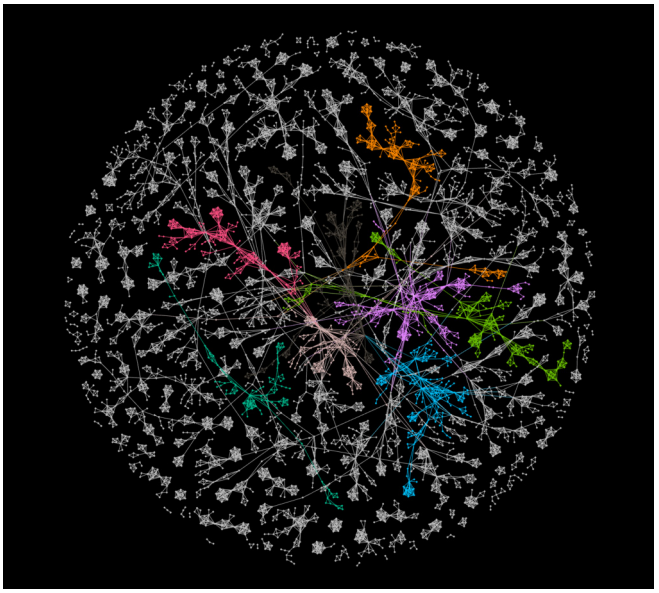

FIG. 3. An example of the nanonetwork transformed by removal of defect bonds; it is grown by aggregation of cliques in the range $n \in [2, 10]$ by chemical affinity $\nu = -5$ (clique repulsion conditions) and the probability of defect bond $p = 0.7$ and $N_{\max} = 5000$ nodes. Different colors of nodes indicate formation of communities.

TABLE I. Graph measures of the assemblies of simplexes of size $n \in [2, 10]$ distributed as $\approx n^{-2}$ and the probability of a defect bond p, for three representative values of the affinity parameter $\nu = \pm 5$ and 0. The properties of graphs with removed pattern of defect edges (0.7-rm) and the graph when the same number of edges c is removed at random (rand-c) are also shown. The effective concentration of defect edges c, the average degree $\langle k \rangle$, the path length $\langle \ell \rangle$, the clustering coefficient $\langle Cc \rangle$, the graph's modularity mod, and the diameter D are computed for the graph size with $N_{\max} = 5000$ nodes. Additional properties computed for the graphs of the same parameters but with $N_{\max} = 1000$ are the hyperbolicity $\delta(G)$ [the largest $\delta_{\max}(d_{\min})$], the topology level q^* at which the connectivity (third structure vector, TSV) between the simplexes drops to zero, and the connectivity at the level $q^* - 1$.

ν	p	c	$\langle k \rangle$	$\langle \ell \rangle$	$\langle Cc \rangle$	mod	D	$\delta(G)$	q^*	TSV($q^* - 1$)
+5	0.0	0	5.005	4.475	0.601	0.524	18	1	9	0.057
	0.7	0.271	5.115	4.197	0.602	0.556	19	1	9	0.435
	0.7-rm	0	5.0671	3.025	0.774	0.414	11	2.0	9	0.160
	rand-c	0	4.162	3.971	0.492	0.517	14	3.0	6	0.079
0	0.0	0	5.988	6.209	0.714	0.882	17	1	8	0.0285
	0.7	0.149	5.933	6.256	0.721	0.872	17	1	7	0.0298
	0.7-rm	0	6.124	5.719	0.742	0.867	17	3.0	8	0.141
	rand-c	0	5.231	7.027	0.610	0.883	23	3.0	7	0.024
−5	0.0	0	5.075	13.213	0.813	0.972	32	1	2	0.005
	0.7	0.109	5.270	11.788	0.825	0.966	27	1	2	0.0129
	0.7-rm	0	5.223	10.417	0.783	0.975	31	5.5	8	0.185
	rand-c	0	4.625	14.751	0.730	0.973	31	4.5	7	0.218

a particular pattern. These effects are especially pronounced in the case of small cliques, where a defect edge provides a more severe restriction on the binding of the remaining faces. In the case of purely geometrical aggregation, $\nu = 0$, the defect edges at sufficiently large concentration form treelike structures and "highways" through the graph. Consequently, the grown network with defect simplexes is different from the case when the simplexes with equal edges were used (i.e., $p = 0$) (see Table I).

In the following, we employ Q analysis [29,36,37] to quantitatively describe the organization of simplicial complexes in various aggregates grown in the presence of defect bonds, according to Eq. (1) and the above-described defect-bond rules. The results are compared with the case without defects, $p = 0$. With the same approaches, we analyze changes in the structures induced by the removal of the defect bonds.

III. Q ANALYSIS AND IMPACT OF DEFECT BONDS ON THE ARCHITECTURE OF NANONETWORKS

In this context, a simplex of order $q_{\max} = n - 1$ is a full graph of n vertices. In a simplicial complex, two simplexes are q connected if they share a face of order q; i.e., they have at least $q + 1$ shared nodes. The dimension of the considered simplicial complex equals the dimension of the largest clique $q_{\max} + 1$ belonging to that complex. To describe the structure of simplicial complexes at different topology levels $q = 0, 1, 2, \ldots, q_{\max}$, Q analysis uses notation from the algebraic topology of graphs [29,38,39]. Specifically:

(i) The first structure vector (FSV) components $\{Q_q\}$ denote the number of q-connected components.

(ii) The second structure vector (SSV) components $\{n_q\}$ correspond to the number of simplexes of order greater than or equal to q.

(iii) The third structure vector (TSV) component q is determined as $\hat{Q}_q \equiv 1 - Q_q/n_q$ measuring the degree of connectivity at the topology level q among the simplexes of order higher than q.

Using the Bron-Kerbosch algorithm [40] we construct the incidence matrix $\Lambda(G)$ of the graph G, starting from its adjacency matrix. The incidence matrix contains complete information about all present simplexes as well as the vertices that belong to each simplex. Thus the components of these structure vectors can be determined from the corresponding incidence matrix $\Lambda(G)$. Further characterization of the architecture of simplicial complexes is provided by the quantity f_q, which is defined [41] as the number of simplexes and faces at the topology level q.

Furthermore, we compute these topology features for the assembly that remains after the removal of defect bonds. Notice that the removal of the defect bonds changes the structure of the assembly by breaking the simplexes in which such bonds were built in. For example, a defect tetrahedron breaks into two triangles that are attached along the common edge when the defect bond is removed. The effects of the defect bond removal correlate with the size of the original cliques. More precisely, the following rules apply:

(a) A clique of order $q_{\max}$ with a defect bond breaks into two cliques of order $q_{\max} - 1$.

(b) These new cliques are attached along their largest face; that is, they share a face of order $q_{\max} - 2$.

Figures 4 and 5 show these structural properties of a few representative aggregates of simplexes obtained with and without defect bonds. Notably, the aggregation of defect bonds causes faces made of pure bonds to spread, which results in higher values of f_q for a finite concentration of defect bonds p, as compared with $p = 0$. This principle applies, although the values are different, for all aggregates at different values of parameter ν. One should also notice that the highest point of f_q correlates with the number of simplexes that need to be added to complete a given number of vertices, here $N_{\max} = 1000$, which is considerably different for different ν (cf. Fig. 1). With the removal of the defect bonds, generally,

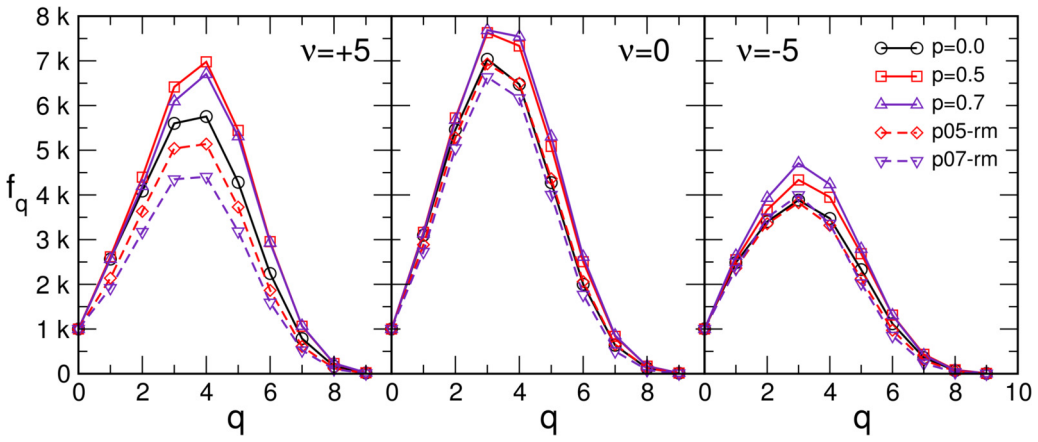

FIG. 4. f_q vs q for the pure ($p = 0$) and defect network ($p = 0.7$, 0.5) and the network obtained by removal of defect bonds (p07-rm, p05-rm) for three values of $\nu = 5, 0, -5$, left to right.

we have a smaller number of simplexes and faces, resulting in the proportional decrease of f_q at all q levels, in comparison with the original structure with defects. The effects are more pronounced in the dense structure of cliques, corresponding to $\nu > 0$ (cf. Fig. 4), than in the structures with sparsely connected cliques (for $\nu < 0$ and partly for $\nu = 0$).

In the structure vectors, shown in Fig. 5, notice that the aggregates grown with or without defect represent one connected component; then the FSV component $Q_0 = 1$. The peak in the FSV at $q = 1$ and the decay at larger $q < 10$ reflects the actual distribution of the size $n \in [2, 10]$ of the attaching cliques; the distribution $f_n \sim n^{-2}$ favors dumbbells as compared with higher-order cliques up to the 10-cliques. The total number of cliques, which is given by the zeroth components of the SSV, given in the middle row in Fig. 5, is significantly more prominent in compact structures ($\nu = +5$) than in the sparse assembly of cliques grown at $\nu = 0$ and $\nu = -5$. This observation is compatible with the growth process depicted in Fig. 1. In the presence of defect cliques, the number of q-connected components, as well as the total number of cliques from the level q upwards, differ from the case of a structure with pure simplexes, in particular in the range of large and intermediate q values. The components of TSV indicate that in the compact regions of the graph (i.e., in the case $\nu = +5$ and partly in $\nu = 0$), the large cliques with defect bonds are more weakly connected than in the pure-simplexes structure. However, in the range $q \in [2, 6]$ for $\nu = +5$ and $q \in [1, 4]$ for the case $\nu = 0$, the connectivity exceeds the curve of TSV for the structure without defects. Meanwhile, in the case $\nu = -5$, the cliques of all sizes share a single node; therefore, they appear to be disconnected already at the level $q = 1$ (cf. TSV in the lower right panel in Fig. 5).

With the removal of defect bonds, the number of large cliques gradually decreases, while the number of intermediate and small cliques results as a balance between breaking the initially present defect cliques of that order and the appearance of new ones from the broken defect cliques of one order higher. Consequently, the FSV changes such that Q_0 increases because of broken bonds; some separate graph parts can occur. The changes are most dramatic in the case of $\nu < 0$. For example, in the structure shown in Fig. 3, some transformed areas of the graph can be recognized as separate communities, while the original modularity is consistent with the individual simplexes. Following a broken bond in a clique of order 9, we have two cliques of order 8 that are sharing a clique of order 7, and so on, as explained above. Consequently, nontrivial connectivity appears among these newly generated cliques at all levels $q \in [1, 8]$, as shown in the lower right panel of Fig. 5, even though the originally built-in cliques repelled each other such to share a single vertex. A similar effect occurs in the sparse areas of the structure grown in the absence of chemical factors ($\nu = 0$). The effects are proportional to the probability of a defect bond p, which decides the actual number of defect bonds in the grown structure, depending on ν (see Table I). In the following, we analyze how the changed architecture of simplicial complexes due to breaking defect bonds affects the hyperbolicity and other features of the topological graph.

IV. CHANGES OF HYPERBOLICITY INDUCED BY THE REMOVAL OF DEFECT BONDS

The hyperbolicity or negative curvature in many complex systems is a measure of closeness of the system's elements that emerges through the evolutionary optimization of their functional properties [2,5,30]. As mentioned in the Introduction, the assembly of cliques possesses a *negative curvature in the graph's metric space*, which is endowed with the shortest-path distance. Hence, the generalized Gromov 4-point hyperbolicity criterion can be applied to characterize it. Specifically, the graph G is hyperbolic if and only if there is an small constant upper bound δ such that, for any four vertices $\{A, B, C, D\}$ of the graph, the relationships between the sums of distances between distinct pairs of these nodes $d(A, B) + d(C, D) \leqslant d(A, C) + d(B, D) \leqslant d(A, D) + d(B, C)$ implies that

$$\delta(A, B, C, D) = \frac{\mathcal{L} - \mathcal{M}}{2} \leqslant \delta. \tag{2}$$

Here $d(U, V)$ indicates the shortest-path distance between U and V and we denoted the largest $\mathcal{L} = d(A, D) + d(B, C)$ and the middle value $\mathcal{M} = d(A, C) + d(B, D)$. We observe that the upper bound of the expression in Eq. (2) is $(\mathcal{L} - \mathcal{M})/2 \leqslant d_{\min}$, where $d_{\min} = \min\{d(A, B), d(C, D)\}$ enables us to determine the graph's hyperbolicity $\delta(G)$ by plotting $(\mathcal{L} - \mathcal{M})/2$

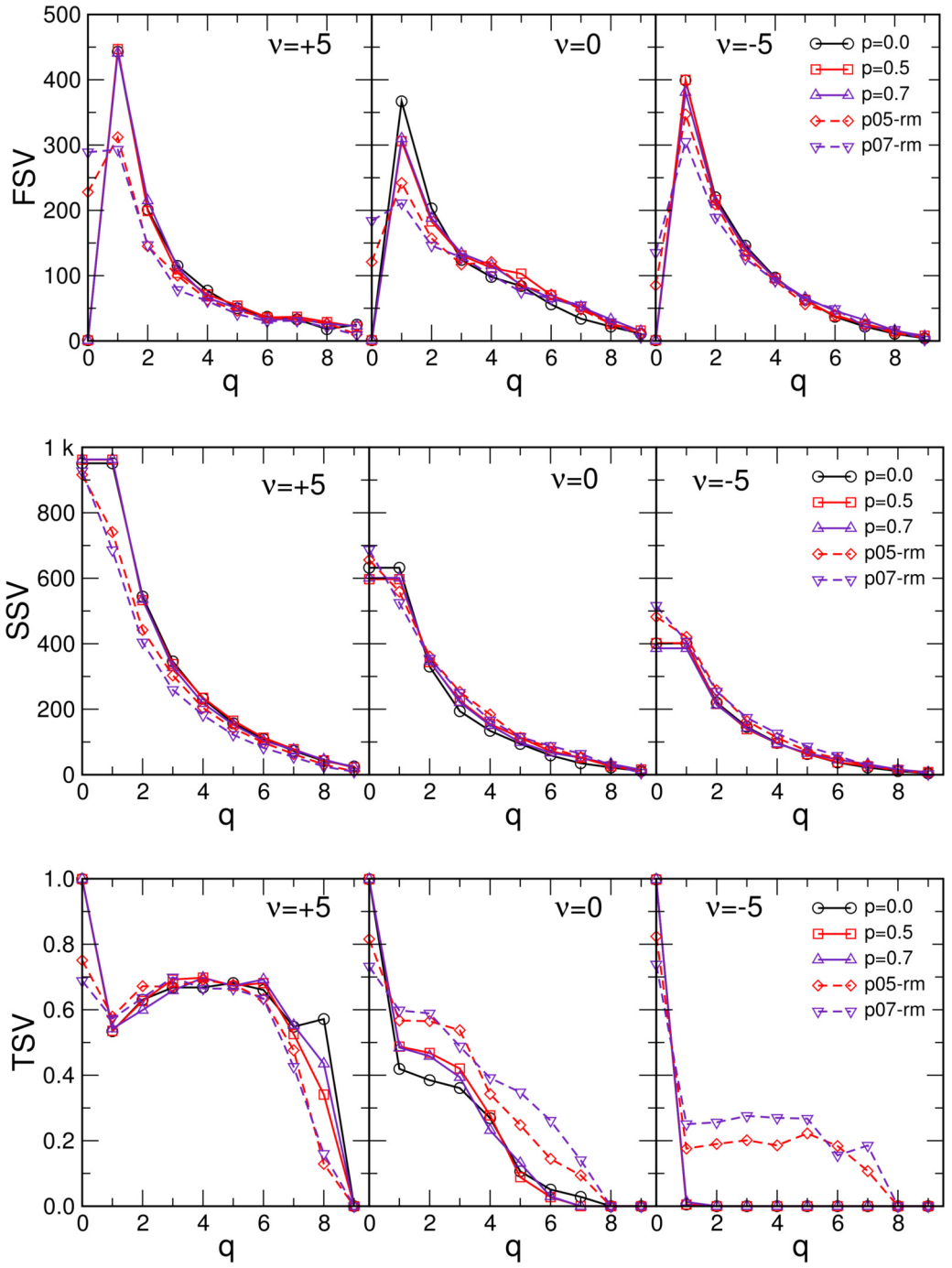

FIG. 5. Components of the first (FSV), second (SSV), and third (TSV) structure vector (top to bottom) against the topology level q for the pure ($p = 0.0$) and defect network ($p = 0.5$ and 0.7) and the network obtained by removal of defect bonds (p05-rm, p07-rm) for three values of $\nu = 5, 0, -5$, indicated on each panel.

against $d_{\min}$ and investigating the worst case, i.e., $\delta_{\max}(d_{\min})$ growth of the dependence. Specifically, for each graph, using its adjacency matrix, we first compute the matrix of distances between all pairs of nodes. Then, by sampling a large number of sets of nodes for the 4-point condition (2) we determine and plot only the largest δ against the corresponding distance $d_{\min}$; then the largest observed value of $\delta_{\max}$ for all $d_{\min}$ in the graph determines the graph's hyperbolicity parameter $\delta(G)$.

For the graphs with a small hyperbolicity parameter, it is known [32,34,42] that the upper bound of the hyperbolicity parameter is related to a specific subjacent structure; for example [43], the presence of an isometric cycle C_n of length $n \geqslant 3$ would lead to $\delta(C_n) = \lfloor n/4 \rfloor - \frac{1}{2}$, if $n \equiv 1(\text{mod}4)$, else $\delta(C_n) = \lfloor n/4 \rfloor$. Similarly, since the cliques are ideally hyperbolic ($\delta_{\text{clique}} = 0$), a combination of cliques that are apart at a small distance i causes the increase of the hyperbolicity parameter by an integer [34], i.e., $\delta_{\text{clique}} + i$.

The network growth in our algorithm by attaching a new clique such that it shares a face with another previously present clique in the system immediately implies that their

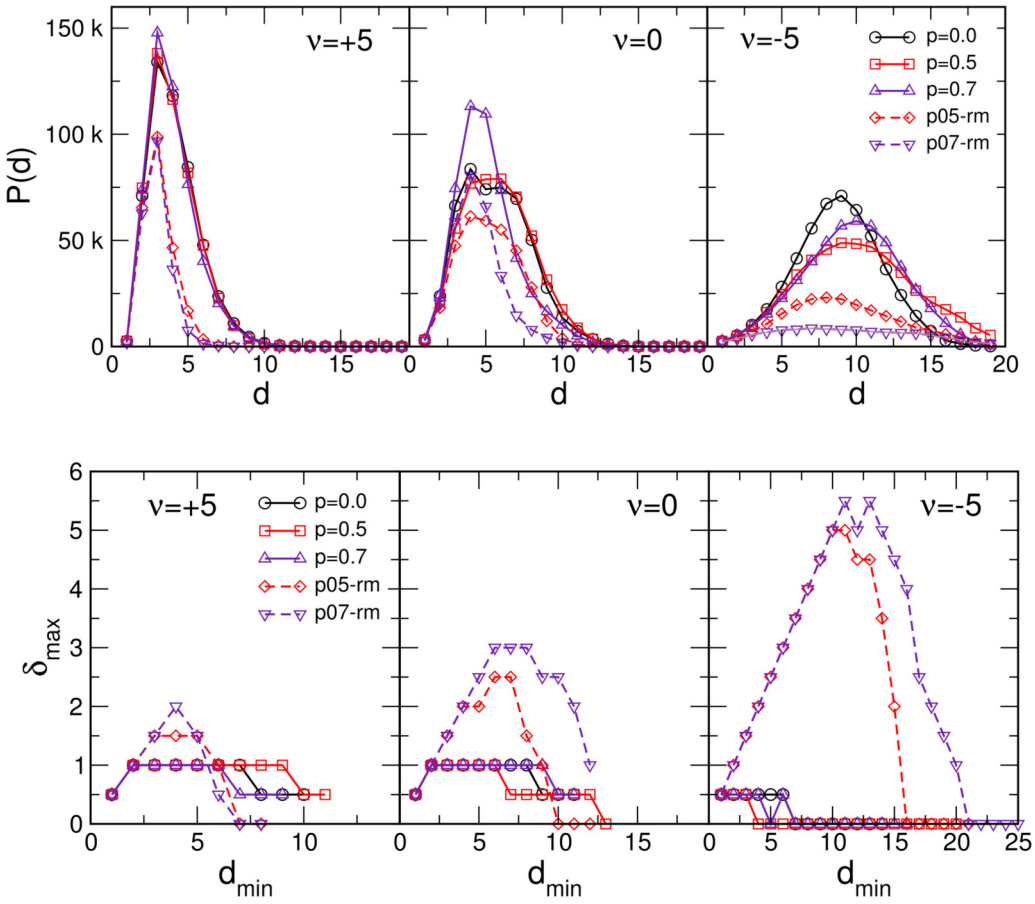

FIG. 6. The distance distribution $P(d)$ vs d, and $\delta_{\max}$ vs $d_{\min}$ for the pure ($p = 0$) and defect network ($p = 0.7, 0.5$) and the network obtained by removal of defect bonds (p05-rm, p07-rm) for three values of $\nu = 5, 0, -5$, left to right.

hyperbolicity parameter cannot exceed unity. That is, these are 1-hyperbolic graphs [25], as also confirmed by a direct computation (see Fig. 6). The same conclusion also applies to the structure grown with the defect cliques, as long as the cliques are complete. However, by removing the defect bonds, the cliques that contained them break into smaller cliques that appear to be differently attached to the rest of the graph. The process often leads to greater distances between the newly apparent cliques. Consequently, an increase of the hyperbolicity parameter $\delta_{\max}$ of the entire graph is observed, as shown for different assemblies in Fig. 6. The lower panels show the hyperbolicity parameter $\delta_{\max}$ for the corresponding graphs. As expected, $\delta_{\max} = 1$ for all graphs grown by the attachment of cliques rule with and without defect bonds, for all ν values. However, when the defect bonds are removed, the changed organization of simplexes, as described above, leads to the increased values of $\delta_{\max}$. The increase strongly depends on the chemical affinity ν at which the graph with defect simplexes is grown. More precisely, in compact structures grown with $\nu > 0$, the hyperbolicity parameter reaches the values $3/2$ or 2, compatible with the subjacent structures with increased distances between the cliques. On the other hand, a substantial increase of $\delta_{\max}$ in the sparse structures reaches the values 3 for $\nu = 0$ and 5.5 for $\nu = -5$ for the considered distribution of clique sizes and concentration of the removed bonds. The increase of the graph's hyperbolicity indicates that, after removal of defect bonds, specific local structures appear that are compatible with the increased distances between vertices. Consequently, they can affect the functional features of the reorganized graphs, as discussed below.

The corresponding top panels of Fig. 6 show the distribution of distances in the case of pure simplexes and in the presence of defect cliques, and how it changes by the removal of defect bonds for varied parameters p and ν. Notice that the distribution of distances between pairs of nodes changes due to the presence of defect bonds. In contrast to the dense graphs (for $\nu = +5$), where the most probable distance remains 3, in the sparse graphs (at $\nu = 0$ and especially at $\nu = -5$) the most probable distances are larger than in the case without defects. Similarly, these graphs experience the most dramatic changes in the distance distributions when the defect bonds are removed. The diameter of the graph (referring to the largest connected component) also changes (cf. Table I).

V. SUMMARY AND DISCUSSION

We have introduced a model for self-assembly of simplexes in the presence of a defect bond and demonstrated the use of embedded defect bonds to reshape the grown structure systematically. The model allows for the variation of the probability of a defect bond in the attaching simplexes in conjunction with their size n and the chemical affinity ν, leading to a wide variety of resulting assemblies. In this study, we consider a fixed probability p and the sizes distributed in the range

$n \in [2, 10]$ according to $p_n \sim n^{-\alpha}$ with $\alpha = 2$. The presence of defect bonds conditions the clique-attachment rules. We adopt the mechanism that favors attachment through straight edges, leading to a treelike pattern of defects. Besides the variation of the size of building cliques n and the parameters α and ν that govern the process (see a demonstration at the link in Ref. [27]), this model also allows other mechanisms for the faces with defect bonds to participate in the process of self-assembly. For example, the possibility of docking between faces with defect edges may lead to a structure where the removal of defects leads to a reshaped assembly with holes. Exploring such structures requires a different topological analysis, which we leave for further work.

We have shown how the presence of defect bonds can tune the structure of simplicial complexes as well as the underlying topological graph. The results of the quantitative analysis in Figs. 4–6 show that the model provides the framework to grow a rich structure of simplicial complexes with the possibility both to control the process of the growth of the assembly as well as to change it by influencing the defect edges after the growth is completed. In this study, we have demonstrated how the removal of defect bonds leads to a hierarchically transformed structure of simplicial complexes and the associated increase of the graphs hyperbolicity parameter. Some standard graph properties and their hyperbolicity as well as measures indicating the connectivity between simplexes are listed in Table I for the representative sets of parameters.

Remarkably, the defect bonds make nonrandom patterns—treelike structures in the graphs—even though no long-range forces are present. The apparent attraction among defects is primarily related to the geometrical constraints for the docking of simplexes; thus, it depends on the size of simplexes and the chemical affinity towards new vertices. Therefore, the removal of patterns of defect bonds has a profound effect on the structure of simplicial complexes, as discussed above. These patterns also shape the graph's properties differently, as compared with the case when the same number of defect bonds are randomly distributed (cf. Table I).

The diversity of the architecture of simplicial complexes, which is enabled by varying the model parameters as well as by the hierarchical reconstruction of the graph after removal of defect bonds, can greatly affect the dynamical processes on these networks [44]. In particular, for diffusion and synchronization processes, the decisive property of the underlying structure is captured by the spectral dimension d_s of the graph. For the assemblies grown with our model without defects, it was shown in Ref. [45] that the spectral dimension $d_s(\nu)$ systematically increases with the chemical affinity parameter ν, and meets the conditions for full synchronization and transient random walks when $\nu > 0$ in association with the increased clique's size. In Ref. [46], a similar conclusion was found for another class of self-assembled simplexes. Recently, in Ref. [47] we have investigated the field-driven magnetization reversal processes on a class of assemblies grown by the present model with defects and $\nu = 0$. The Ising spins are attached to the nodes (nanoparticles) of the assembly having antiferromagnetic interactions through the defect bond. Meanwhile, the remaining interactions are ferromagnetic. In this case, the underlying structure provides geometric frustration effects. Hence, for these processes, the occurrence of frustrated triangles as faces of different simplexes is of primary importance. On the other hand, larger structures, simplicial complexes, and mesoscopic communities play a key role in the synchronization and diffusion processes. Notably, a defect edge in an n-clique induces $n - 2$ frustrated triangles that are built in a simplicial complex. It was shown [47] that different sizes of cliques that comprise simplicial complexes directly influence the shape of the hysteresis loop and the occurrence of plateaus at fractional magnetization levels. Such plateaus are similar to those observed in disordered antiferromagnetic materials of a complex morphology [48,49]. For example, in the graphs in Figs. 1(a) and 1(b), the original tetrahedra disappear after removal of defect bonds. The remaining graphs consist of triangles and edges. Hence, in the case of antiferromagnetic interactions between spins on these structures, the hysteresis loop will split into two parts. This shape is in contrast to the loop on the original structures with tetrahedra, which has a compact central part (cf. Fig. 3 in Ref. [47]). Based on the results of the hysteresis loop [47] and the theory of cooperative phenomena on complex networks [44], we expect that the different architectures of simplicial complexes grown by our model as well as their hierarchical reconstruction by the removal of defect bonds readily affect the spin response function in these assemblies. Investigations of spin reversal processes are in progress in the assemblies grown by the present model with defect bonds and various other parameters.

In summary, we have introduced classes of nanonetworks that evolve by self-assembly of formatted groups of nodes as simplexes with different shapes and types of bonds. The variations of the parameters governing the process of self-assembly allow different types of structures to grow from sparsely separated simplexes to compact structures with large simplicial complexes, and the possibility to modify their organization by affecting a specific type of bond. These approaches are suitable for designing new classes of nanostructured assemblies and for their quantitative characterization beyond the standard pairwise interactions. In this context, our model provides a mathematical framework for compelling research on new functional properties of such assemblies. The presented study also offers a deeper understanding of the mechanisms beyond the higher-order connectivity that lead to the occurrence of simplicial complexes in many other complex systems, from human connectomes [2] to patterns representing the brain-to-brain coordination [50] and online social dynamics [51,52], as well as a variety of problems in physics [5–7,41,47,53].

ACKNOWLEDGMENTS

Authors acknowledge the financial support from the Slovenian Research Agency under the program P1-0044 and from the Ministry of Education, Science and Technological Development of the Republic of Serbia.

[1] B. Tadić, V. Gligorijević, M. Mitrović, and M. Šuvakov, Co-evolutionary mechanisms of emotional bursts in online social dynamics and networks, Entropy **15**, 5084 (2013).

[2] B. Tadić, M. Andjelković, and R. Melnik, Functional geometry of human connectomes, Sci. Rep. **9**, 12060 (2019).

[3] J. Živković and B. Tadić, Nanonetworks: The graph theory framework for modeling nanoscale systems, NanoMMTA **2**, 30 (2013).

[4] S. Ikeda and M. Kotani, *A New Direction in Mathematics for Materials Science* (Springer, Tokyo, 2015).

[5] G. Bianconi, C. Rahmede, and Z. Wu, Complex quantum network geometries: Evolution and phase transitions, Phys. Rev. E **92**, 022815 (2015).

[6] N. Cinardi, A. Rapisarda, and G. Bianconi, Quantum statistics in network geometry with fractional flavor, J. Stat. Mech. (2019) 103403.

[7] B. Tadić, M. Andjelković, and M. Šuvakov, The influence of architecture of nanoparticle networks on collective charge transport revealed by the fractal time series and topology of phase space manifolds, J. Coupled Syst. Multiscale Dyn. **4**, 30 (2016).

[8] S. V. Krivovichev, Combinatorial topology of salts of inorganic oxoacids: Zero-, one- and two-dimensional units with corner-sharing between coordination polyhedra, Crystallogr. Rev. **10**, 185 (2004).

[9] B. Pelaz *et al.*, The state of nanoparticle-based nanoscience and biotechnology: Progress, promises, and challenges, ACS Nano **6**, 8468 (2012).

[10] X. Fan, J. Y. Chung, Y. X. Lim, Z. Li, and X. J. Loh, Review of adaptive programmable materials and their bioapplications, ACS Appl. Mater. Interfaces **8**, 33351 (2016).

[11] G. M. Whitesides and B. Grzybowski, Self-assembly at all scales, Science **295**, 2418 (2002).

[12] X. Xing, J. Wang, X. Kuang, X. Xia, C. Lu, and G. Maroulis, Probing the low-energy structures of aluminum-magnesium alloy clusters: A detailed study, Phys. Chem. Chem. Phys. **18**, 26177 (2016).

[13] M. A. Boles, M. Michael Engel, and D. V. Talapin, Self-assembly of colloidal nanocrystals: From intricate structures to functional materials, Chem. Rev. **116**, 11220 (2016).

[14] W. Li and M. Müller, Defects in the self-assembly of block copolymers and their relevance for directed self-assembly, Annu. Rev. Chem. Biol. Eng. **6**, 187 (2015).

[15] T. Harada and A. Hatton, Formation of highly ordered rectangular nanoparticle superlattices by the cooperative self-assembly of nanoparticles and fatty molecules, Langmuir **25**, 6407 (2009).

[16] D. R. Hickey, R. J. Wu, J. S. Lee, J. G. Azadani, R. Grassi, D. C. Mahendra, J.-P. Wang, T. Low, N. Samarth, and K. A. Mkhoyan, Large-scale interlayer rotations and Te grain boundaries in $(Bi, Sb)_2Te_3$ thin films, Phys. Rev. Materials **4**, 011201(R) (2020).

[17] S. Ikeda and M. Kotani, Materials inspired by mathematics, Sci. Technol. Adv. Mater. **17**, 253 (2016).

[18] M. Šuvakov and B. Tadić, Collective charge fluctuations in single-electron processes on nanonetworks, J. Stat. Mech.: Theory Exp. (2009) P02015.

[19] M. O. Blunt, M. Šuvakov, F. Pulizzi, C. P. Martin, E. Pauliac-Vaujour, A. Stannard, A. W. Rushforth, B. Tadic, and P. Moriarty, Charge transport in cellular nanoparticle networks: Meandering through nanoscale mazes, Nano Lett. **7**, 855 (2007).

[20] M. O. Blunt, A. Stannard, E. Pouliac-Vaujour, C. P. Martin, I. Vancea, M. Suvakov, U. Thiele, B. Tadic, and P. Moriarty, Patterns and pathways in nanoparticle self-organization, in *Oxford Handbook of Nanoscience and Technology: Volume 1: Basic Aspects*, edited by V. A. Narlikar and Y. Y. Fu (Oxford University Press, Oxford, 2010), pp. 214–248.

[21] M. Šuvakov and B. Tadić, Modeling collective charge transport in nanoparticle assemblies, J. Phys.: Condens. Matter **22**, 163201 (2010).

[22] Y. Gu, R. Burtovyy, J. Townsend, J. R. Owens, I. Luzinov, and K. G. Kornev, Collective alignment of nanorods in thin newtonian films, Soft Matter **9**, 8532 (2013).

[23] S. Ahn and S. J. Lee, Hierarchical nanoparticle clusters induced by block copolymer self-assembly, Soft Matter **10**, 3897 (2014).

[24] S. Liu and J. Yu, Cooperative self-construction and enhanced optical absorption of nanoplates-assembled hierarchical Bi_2Wo_6 flowers, J. Solid State Chem. **181**, 1048 (2008).

[25] M. Šuvakov, M. Andjelković, and B. Tadić, Hidden geometries in networks arising from cooperative self-assembly, Sci. Rep. **8**, 1987 (2018).

[26] Y. Wang, Y. Wang, D. R. Breed, V. N. Manoharan, L. Feng, A. D. Hollingsworth, M. Weck, and D. J. Pine, Colloids with valence and specific directional bonding, Nature **491**, 51 (2012).

[27] M. Šuvakov, M. Andjelković, and B. Tadić, Applet: Simplex aggregated growing graph, http://suki.ipb.rs/ggraph/ (2017).

[28] J. Jonsson, *Simplicial Complexes of Graphs*, Lecture Notes in Mathematics (Springer-Verlag, Berlin, 2008).

[29] J. R. Beaumont and A. C. Gatrell, *An Introduction to Q-Analysis*, Geo Abstracts (Edmund Nome Press, Norwich, 1982).

[30] D. Krioukov, F. Papadopoulos, M. Kitsak, A. Vahdat, and M. Boguna, Hyperbolic geometry of complex networks, Phys. Rev. E **82**, 036106 (2010).

[31] J. M. Rodriguez and E. Touris, Gromov hyperbolicity through decomposition of metric spaces, Acta Math. Hung. **103**, 53 (2004).

[32] S. Bermudo, J. M. Rodríguez, O. Rosario, and J. M. Sigarreta, Small values of the hyperbolicity constant in graphs, Discrete Math. **339**, 3073 (2016).

[33] S. Bermudo, J. M. Rodríguez, J. M. Sigarreta, and J. M. Vilaire, Gromov hyperbolic graphs, Discrete Math. **313**, 1575 (2013).

[34] N. Cohen, D. Coudert, G. Ducoffe, and A. Lancin, Applying clique-decomposition for computing Gromov hyperbolicity, Theor. Comput. Sci. **690**, 114 (2017).

[35] M. Šuvakov and B. Tadić, Topology of cell-aggregated planar graphs, in *Computational Science—ICCS 2006*, edited by V. N. Alexandrov, G. D van Albada, P. M. A. Sloot, and J. Dongarra (Springer, Berlin, 2006), pp. 1098–1105.

[36] H. J. Bandelt and V. Chepoi, Metric graph theory and geometry: A survey, in *Surveys on Discrete and Computational Geometry: Twenty Years Later*, edited by J. E. Goodman, J. Pach, and R. Pollack (American Mathematical Society, Providence, RI, 2008), Vol. 453.

[37] S. Maletić and Y. Zhao, *Simplicial Complexes in Complex Systems: The Search for Alternatives* (Harbin Institute of Technology, Harbin, China, 2017).

[38] R. H. Atkin, An algebra for patterns on a complex, II, Int. J. Man-Mach. Stud. **8**, 483 (1976).

[39] J. Johnson, Some structures and notation of Q-analysis, Environ. Plann. B: Plann. Des. **8**, 73 (1981).

[40] C. Bron and J. Kerbosch, Finding all cliques of an undirected graph, Commun. ACM **16**, 575 (1973).

[41] M. Andjelković, N. Gupte, and B. Tadić, Hidden geometry of traffic jamming, Phys. Rev. E **91**, 052817 (2015).

[42] W. Carballosa, D. Pestana, J. M. Rodríguez, and J. M. Sigarreta, Distortion of the hyperbolicity constant in minor graphs, Electron. Notes Discrete Math. **46**, 57 (2014).

[43] Y. Wu and C. Zhang, Hyperbolicity and chordality of a graph, Electron. J. Combinatorics **18**, P43 (2011).

[44] S. N. Dorogovtsev, A. V. Goltsev, and J. F. F. Mendes, Critical phenomena in complex networks, Rev. Mod. Phys. **80**, 1275 (2008).

[45] M. Mitrović Dankulov, B. Tadić, and R. Melnik, Spectral properties of hyperbolic nanonetworks with tunable aggregation of simplexes, Phys. Rev. E **100**, 012309 (2019).

[46] A. P. Millán, J. J. Torres, and G. Bianconi, Synchronization in network geometries with finite spectral dimension, Phys. Rev. E **99**, 022307 (2019).

[47] B. Tadić, M. Andjelković, M. Šuvakov, and G. J. Rodgers, Magnetisation processes in geometrically frustrated spin networks with self-assembled cliques, Entropy **22**, 336 (2020).

[48] Y. I. Dublenyich, Ground States of the Ising Model on the Shastry-Sutherland Lattice and the Origin of Fractional Magnetization Plateaus in Rare-Earth-Metal Tetraborides, Phys. Rev. Lett. **109**, 167202 (2012).

[49] D. Brunt, G. Balakrishnan, D. Mayoh, M. R. Lees, D. Gorbunov, N. Qureshi, and O. A. Petrenko, Magnetisation processes in the rare earth tetraborides NdB_4 and HoB_4, Sci. Rep. **8**, 232 (2018).

[50] B. Tadić, M. Andjelković, B. M. Boshkoska, and Z. Levnajić, Algebraic topology of multi-brain connectivity networks reveals dissimilarity in functional patterns during spoken communications, PLoS One **11**, e0166787 (2016).

[51] M. Andjelković, B. Tadić, S. Maletić, and M. Rajković, Hierarchical sequencing of online social graphs, Physica A (Amsterdam, Neth.) **436**, 582 (2015).

[52] M. Andjelković, B. Tadić, M. Mitrović Dankulov, M. Rajković, and R. Melnik, Topology of innovation spaces in the knowledge networks emerging through questions-and-answers, PLoS One **11**, e0154655 (2016).

[53] B. Senyuk, Q. Liu, E. Bililign, P. D. Nystrom, and I. I. Smalyukh, Geometry-guided colloidal interactions and self-tiling of elastic dipoles formed by truncated pyramid particles in liquid crystals, Phys. Rev. E **91**, 040501(R) (2015).